BULLETIN OF THE POLISH ACADEMY OF SCIENCES
TECHNICAL SCIENCES, Vol. 73(5), 2025, Article number: e155040
DOI: 10.24425/bpasts.2025.155040

Experimental testing of a rocket motor thrust vector control actuation system demonstrator

Łukasz Krzysztof NOCOŃ* **and Piotr Krzysztof SZMIDT**

Kielce University of Technology, Department of Mechatronics and Armament Engineering, Faculty of Mechatronics and Mechanical Engineering, al. Tysiąclecia Państwa Polskiego 7, 25-314 Kielce, Poland

Abstract. This paper presents the results of simulation and experimental studies concerning the control of a rocket motor thrust vector direction. The change in direction was achieved using a developed and constructed control actuation system demonstrator. The first part of the article focuses on presenting the demonstrator for a hypothetical rocket missile equipped with this system and simulations of the missile flight control. Simulation results determined the required thrust vector deflection angles. Subsequently, this data was used to program the control actuation system (CAS) and conduct experiments on the physical demonstrator. By commanding specific deflections of the actuator system over time, the resulting forces and moments were measured during thrust generation, simulating flight scenarios for approximately 8 seconds. The results indicate that the proposed actuator system performs its function effectively, deflecting the thrust vector largely in line with simulation predictions, after adopting system efficiency coefficients. The novelty of this work lies in comparing real-time actuator testing with a simulation control for subsonic ATGMs and finding deflection efficiency coefficients to improve the simulation model.

Keywords: anti-tank missile; thrust vectoring control; control actuation system; experimental testing.

1. INTRODUCTION

Missile control systems are one of the essential parts for achieving high precision and maneuverability, especially in dynamically changing battlefield conditions. These systems enable guided missiles to engage diverse targets, both stationary and mobile, under various atmospheric and operational constraints. Control methods vary depending on the missile type, flight regime, and mission objectives. The most common actuation strategies include aerodynamic control surfaces (e.g., fins, canards), thrust vector control (TVC), and reaction control systems (RCS).

Aerodynamic surfaces are traditionally favored for high-speed missiles operating within the atmosphere, such as anti-aircraft interceptors. Their effectiveness, however, diminishes at lower speeds or high altitudes due to a reduction in dynamic pressure, which scales with the square of flight velocity and air density. In such regimes, alternative control strategies like TVC become indispensable.

Thrust vector control offers a compelling solution, particularly during the missile terminal and finishing phases, where rapid response and high precision are needed. Jet vane-based TVC systems, in which vanes are inserted into the nozzle flow to deflect exhaust and generate control moments, have been the subject of extensive research. Murty *et al.* [1, 2] conducted detailed numerical simulations to characterize the flow fields and control performance of jet vane configurations, revealing important insights into their efficiency and thrust losses. Majil *et al.* [3] further explored design optimizations aimed at minimizing performance penalties associated with vane-induced shockwaves. Practical implementations of jet vane systems are documented in patent literature, such as Kim *et al.* [4], where integrated actuation mechanisms were developed for enhanced responsiveness. Meanwhile, Shin and Kim [5] introduced a dual throat nozzle approach, improving control authority by exploiting pressure differentials. Fluidic thrust vectoring via secondary fluid injection has also garnered attention, as shown by Chouicha *et al.* [6], who investigated the effects of reactive gases on deflection efficiency. Complementary work by Forde *et al.* [7] introduced the thrust augmentation nozzle (TAN), combining structural and fluidic strategies to enhance booster performance.

Innovative TVC concepts have emerged, including shock-vector control in axisymmetric nozzles as proposed by Resta *et al.* [8], and transverse gas injection techniques studied by Zmijanovic *et al.* [9], both expanding the theoretical framework, although for supersonic TVC. Experimental insights by Isaac and Rajashekar [10] highlighted the operational feasibility of fluidic TVC systems, while Harris and Slegers [11] demonstrated that TVC could sustain control performance even under aerodynamic surface damage, reinforcing its value in combat resilience. The work [12] focuses on heat transfer and heat resistance on jet tabs in TVC systems, which is also a key issue, as materials used must meet specific requirements to maintain proper missile control.

For subsonic applications such as anti-tank guided missiles (ATGMs), which typically operate around 250 m/s and must hit small, mobile, and often armored targets, TVC offers considerable benefit. These missiles often utilize advanced guid-

*e-mail: lnocon@tu.kielce.pl

Manuscript submitted 2025-05-02, revised 2025-07-07, initially accepted for publication 2025-07-14, published in November 2025.

© 2025 The Author(s). This is an open access article under the CC BY license (http://creativecommons.org/licenses/by/4.0/)

ance schemes, such as semi-automatic command to line of sight (SACLOS) or "fire-and-forget" technologies and may incorporate top-attack profiles to defeat modern armor. In such systems, aerodynamic controls alone are insufficient to achieve the desired agility, making hybrid control strategies appealing.

This study builds upon prior work on a hypothetical subsonic ATGM platform. Nocoń *et al.* [13] developed a detailed physical and mathematical model of this missile, employing a modified linear quadratic regulator (mLQR) for trajectory stabilization. The mLQR technique, an evolution from PID and classical LQR controllers, incorporates time-varying system dynamics via Jacobian matrices, enabling improved real-time adaptability. Comparative studies have explored alternative LQR approaches, including hybrid [14], fuzzy [15–17], and switched LQR schemes [18, 19], each contributing to robustness in different operational scenarios. Bużantowicz [20] provided a systematic methodology for tuning LQR gain matrices, offering an analytical framework adaptable to varying mission profiles. Further applications of LQR in missile roll and pitch control were explored by Kantubhukta *et al.* [21].

The integrated control concept, combining aerodynamic surfaces with TVC, was introduced and preliminarily validated by Nocoń and Koruba [22–24]. A physical TVC demonstrator featuring a movable nozzle with optional jet vanes was constructed and evaluated under the Polish NCBR-funded project [25]. This paper extends that work by validating simulation predictions against experimental measurements obtained from this demonstrator.

In the present study, we use custom-built simulation tools to model flight dynamics and compute control commands. These angular deflections serve as reference inputs to the physical demonstrator, enabling a direct comparison between simulated and real-world actuator responses. The primary objective is to assess whether the developed TVC mechanism can replicate simulation-predicted control moments, thereby confirming its viability for future ATGM integration.

2. MODEL OF A HYPOTHETICAL ANTI-TANK GUIDED MISSILE

The controlled plant is a subsonic, hypothetical anti-tank guided short or medium-range missile of the "fire and forget" type (Fig. 1). Its in-flight control is achieved through a double control actuation system, which consists of two pairs of aerodynamic controls (rudders and elevators) in the front section of the missile and a tilting missile engine nozzle in the rear section (Fig. 2). The tilting nozzle changes the angular position of the rocket engine thrust vector resultant relative to the missile longitudinal axis Sx. While in the paper [26], the authors proposed dual-control missiles that have sets of aerodynamic fins both in front of and behind the missile center of mass, in this paper, we consider the hybrid control actuation system (hCAS) consisting of aerodynamic surfaces and a moving rocket motor nozzle constituting the essence of the research of this article. The application of a hybrid control actuation system significantly improves missile maneuverability, which was reviewed in the article [23].

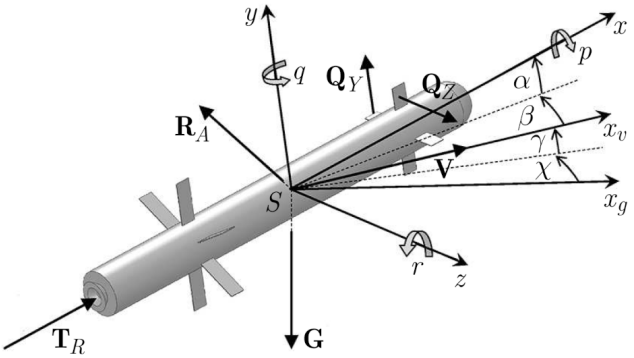

Fig. 1. Force system acting on the ATGM within the gravitational field and Earth's atmosphere, together with the accepted coordinate systems

Figure 1 uses the following symbols and designations: $\mathbf{G}$ – force of gravity; $\mathbf{R}_A$ – vector of resultant aerodynamic forces; $\mathbf{Q}_Y$, $\mathbf{Q}_Z$ – control forces; $\mathbf{T}_R$ – engine thrust; $\mathbf{V}$ – vector of missile velocity; $Sx_gy_gz_g$ – ground-fixed coordinate system; $Sx_vy_vz_v$ – coordinate system connected with the flow; $Sxyz$ – coordinate system connected with the missile; α – angle of attack; β – missile sideslip angle; γ and χ – angles of the velocity vector (flight-path angles); p, q, r – angular velocity components in the body-fixed system.

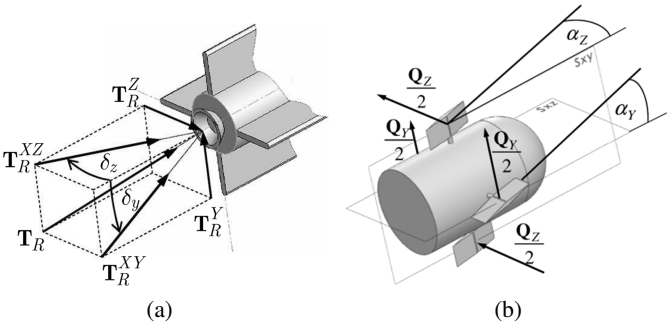

(a) (b)

Fig. 2. Generation of control forces while (a) tilting the engine nozzle; (b) deflection angles of aerodynamic control surface

Figure 2 uses the following symbols and designations: $\mathbf{T}_R$ – engine thrust; $\mathbf{T}_R^Y$ – thrust projection on the vertical axis Sy; $\mathbf{T}_R^Z$ – thrust projection on the horizontal axis Sz; $\mathbf{T}_R^X$ – thrust projection on the longitudinal axis of the ATGM Sx; $\mathbf{T}_R^{XY}$ – thrust projection on the vertical plane Sxy; $\mathbf{T}_R^{XZ}$ – thrust projection on the horizontal plane Sxz; δ_z, α_Z – control angle in the horizontal plane (change Yaw); δ_y, α_Y – control angle in the vertical plane (change Pitch).

It was assumed that the aerodynamic control surface and rocket motor nozzle deflection angles have the same value but opposite directions. Therefore, we have $\alpha_Y = -\delta_y$ in the vertical plane and $\alpha_Z = -\delta_z$ in the direction control plane, which results in the following formulas:

$$Q_Y = \alpha_Y P_S\,, \qquad T_R^Y \approx -T_R \cdot \alpha_Y\,, \tag{1}$$

$$Q_Z = \alpha_Z P_S\,, \qquad T_R^Z \approx -T_R \cdot \alpha_Z\,, \tag{2}$$

where $P_S = 2S_S\rho\frac{V^2}{2}$, S_S – area of surfaces ($S_S = 0.009$ m^2); ρ – air density ($\rho = 1.225$ kg/m^3); α_Y, α_Z – the actual deflection angles of the aerodynamic control surfaces.

The simulation studies presented in this article are based on a mathematical model, the current version of which is described in detail in [13]. It is recommended to consult earlier publications in which the model was systematically developed. In [24], the process of generating the reference trajectory is described in detail. The core idea of the reference trajectory was to execute a series of obstacle-avoidance maneuvers.

The flight trajectory is divided into several segments between waypoints. Each segment of the reference trajectory is defined as a polynomial function derived from the coordinates of the respective waypoints.

Over time, various control strategies were applied within the model. Initially, a PID controller was used. An analysis of different PID configurations was presented in [27]. Subsequently, attempts were made to implement an LQR controller; however, these required significant simplifications of the mathematical model. As a result, the model became less representative of the real system.

Since the missile is a time-varying dynamic system, it became necessary to introduce time-dependent state matrices A and control matrices B. A modified mLQR controller, adapted to these conditions, was introduced in [28].

3. DEMONSTRATOR

The thrust vector control system demonstrator was developed as part of a project funded by the Polish National Centre for Research and Development (NCBR, grant number DOB-2P/03/04/2018) (Fig. 3). The design is protected by intellectual property rights through a series of six patents [29–34]. A detailed description of the prototype development process is provided in [25], which also includes the results of experimental testing. The purpose of these tests was to verify the design assumptions and assess the technical feasibility of the system.

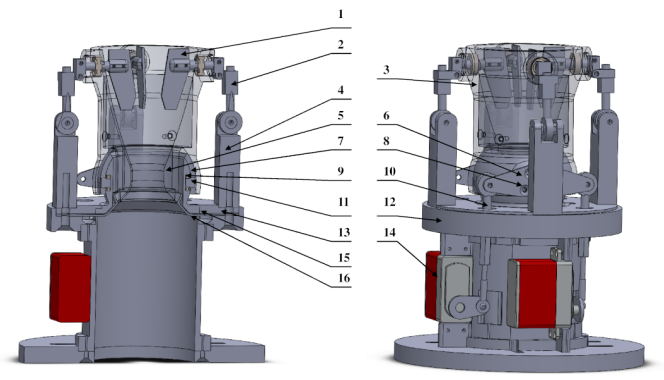

Fig. 3. Side view of the demonstrator thrust vector control system

It was assumed that supplying air at a constant pressure into the pressure chamber would simulate the exhaust gases, i.e., the combustion products of a solid-propellant rocket motor, thus generating control forces and thrust equivalent to those produced by the actual rocket exhaust. A cross-sectional view with labeled components is shown in Fig. 3.

The elements shown in Fig. 3 are as follows:
1 – jet vane; 2 – telescopic connector with the jet vane mount; 3 – diffuser; 4 – support to mount the telescopic connector; 5 – throat insert; 6 – lever to mount the ball joints; 7 – central ring of the gimbal-type joint; 8 – socket to seat the bearing responsible for one axis of rotation of the nozzle; 9 – MR 106 2RS bearing; 10 – ball joint connecting the moveable nozzle and the actuator; 11 – 6 mm diameter pin; 12 – missile body; 13 – frame of the inner ring of the gimbal-type joint with a socket to seat the bearing responsible for the other axis of rotation; 14 – servomechanism FeeTech FT835BL; 15 – heat insulation ring; 16 – elastic sealing cover plate.

The experimental tests were performed using a demonstrator constructed primarily from metals. The main components were made of aluminum using a Hermle B300 five-axis machining center. Exceptions include the central gimbal ring (7) and the telescopic connector rod (2), which were CNC-machined from steel (Fig. 4).

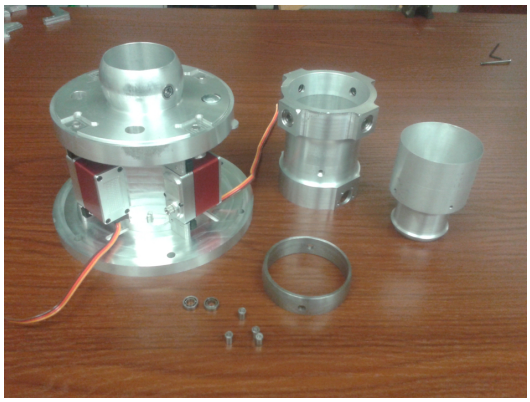

Fig. 4. Aluminum demonstrator with a steel central gimbal ring before the assembly

A partially disassembled view of the demonstrator, with the central gimbal ring visible, is shown in Fig. 4. The fully assembled demonstrator, ready for testing, is presented in Fig. 5.

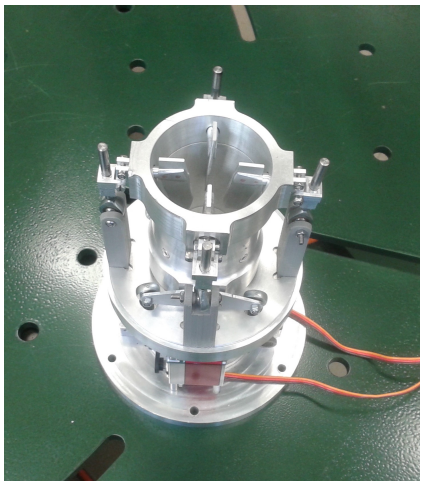

Fig. 5. Demonstrator before the tests

Subsequent figures (Figs. 6 and 7) illustrate the angular deflections of the thrust vector control components and the location of the axes of the MCS10 multi-axis sensor.

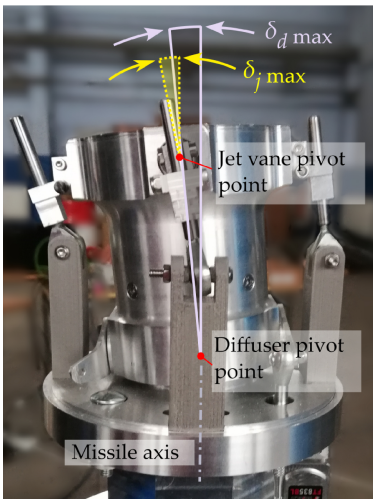

Fig. 6. Metal demonstrator attached to the test rig

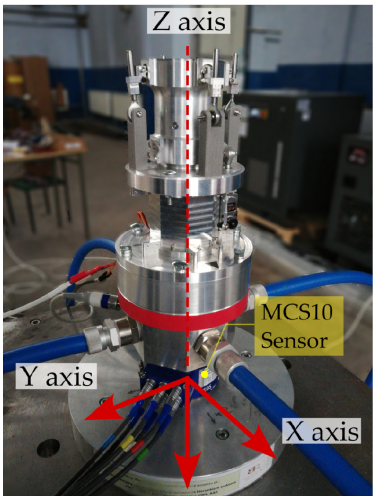

Fig. 7. Metal demonstrator attached to the test rig, orientations of the coordinate axes of the MCS10 multi-axis sensor

A cross-sectional view and the key dimensions of the measurement setup with the mounted demonstrator are shown in Fig. 8.

The main geometric dimensions of the demonstrator were:

- The inlet diameter $D_{\text{in}} = 62.50$ mm
- The outlet diameter $D_{\text{out}} = 60.00$ mm
- The nozzle throat diameter $D_g = 20$ mm
- The combustion chamber length $L_c = 88$ mm
- The length of the convergent section of the nozzle, $L_z = 20$ mm
- The length of the divergent section of the nozzle, $L_r = 80$ mm
- The surface area of the jet vanes (area of control surfaces) $S_T = 1800$ mm^2 (4×450 mm$^2 = 1800$ mm^2)

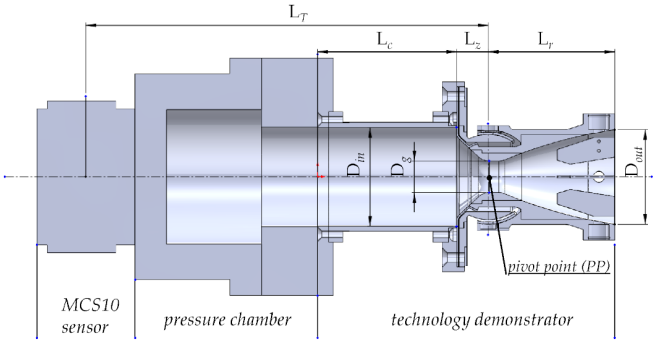

Fig. 8. Geometric model of the technology demonstrator

- The distance of the axis of rotation of the diffuser from the point of measurement (origin of the sensor coordinates), $L_T = 254.5$ mm

4. COMPARISON AND EXPERIMENT EXECUTION

Using the previously discussed mathematical model, a computer simulation of the rocket missile flight was conducted. The flight parameters in the simulation were adjusted to match the capabilities of the demonstrator and the measurement system. The following parameters were assumed:

- An initial mass of 13.287 kg
- A final mass of 8.7 kg (after missile propellant consumption)
- The length of ATGM $l_m = 1.2$ m
- A diameter of 0.12 m
- A launch motor ($0 \leq t < 0.5$ s), and the thrust is 4.3 kN
- A main motor ($0.5 \leq t < 7.5$ s), the thrust of which is 190 N
- Control angles: -10 deg to 10 deg
- Initial velocity of the ATGM $v_0 = 50$ m/s
- Sample time $\mathrm{d}t = 0.001$ s

The article presents two experiments. The experiments were performed for both types of demonstrators, i.e., with and without jet vanes, at an inlet pressure of 0.8 MPa. Each experiment lasts 7.5 seconds, corresponding to the duration of the rocket motor operation in the simulation. The experimental tests were designed based on computer simulations. Angular deviations of the resultant thrust vector, obtained from the simulation, were imported into the control system every 0.02 seconds.

During the first 0.5 seconds of the simulation, the launch motor operates with a thrust of 4300 N. Such forces cannot be replicated on the test bench. Therefore, significant discrepancies observed in this initial phase are disregarded in the analysis.

The tests were conducted using a specially developed test rig equipped with an HBM MCS10 multi-axis force/torque sensor, an HBM P8AP pressure transducer, and an HBM MX840B data acquisition system. Data from the test bench are recorded at a sampling rate of 300 Hz. The peak-to-peak noise floor of the measurement system, approximately 0.3 N for forces, 0.02 Nm for moments, and 0.002 bar for pressure, is negligible, being at least ten times lower than the noise and disturbances caused by air flow during experiments. To mitigate the significant signal noise introduced by air flow, the recorded data were filtered using a moving average filter applied over 10 samples.

4.1. Experiment 1

The first simulation results, presented in Figs. 9 and 10 concern the missile flight for the following parameters: starting target position: $x_{t0} = 1700$ m, $y_{t0} = 5$ m, $z_{t0} = 0$ m; angle of a missile launch: $\gamma_{m0} = 0$ deg, $\chi_{m0} = 0$ deg; starting angle of pitch and yaw of a target velocity vector: $\gamma_{t0} = 0$ deg, $\chi_{t0} = 0$ deg; target velocity: $V_t = 20$ m/s. Missile passing through two waypoints: $P_1(400; 20; 0)$, $P_2(700; 4; 0)$.

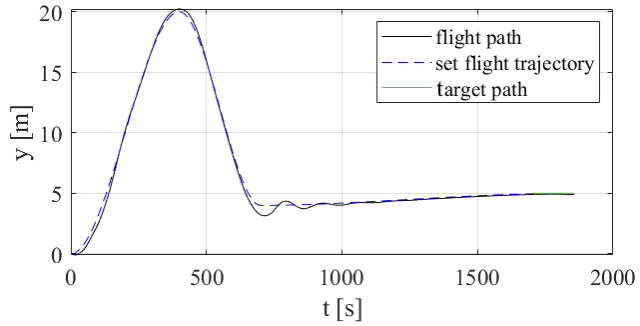

Fig. 9. The performed and set flight trajectory in the vertical plane

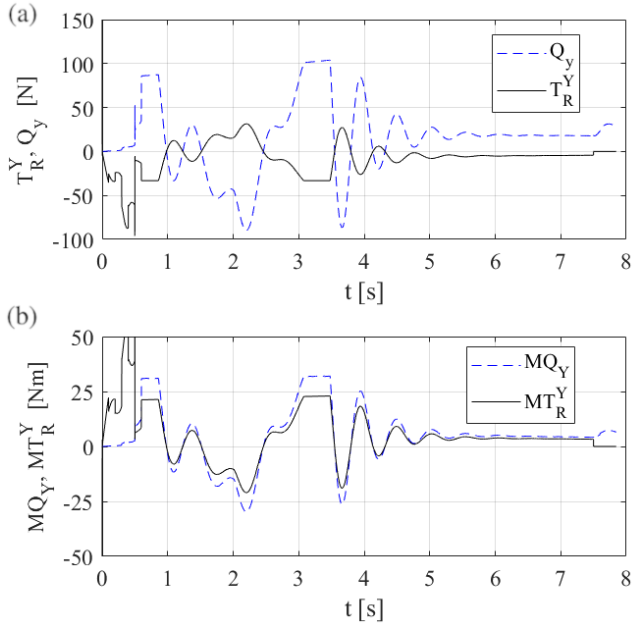

Fig. 10. The performed control forces (a) and moments (b) of the anti-tank guided missile flight in the vertical plane

The following figures present the results of an experiment conducted using angular data obtained from a computer simulation, which were implemented in the actuator control system. The experiment aims to compare the experimental results with those from the computer simulation. The simulation accounts for the mass loss of the ATGM due to rocket fuel consumption. As a result, the moments of inertia, mass, and the position of the center of mass change over the course of the flight.

The distance between the center of mass and the point of application of the thrust vector in the hypothetical ATGM used in the simulation differs from that in the physical experiment. In the simulation, this distance is modeled as a linear function, changing according to the equation: $f(t) = 0.018133t + 0.63$ m, whereas in the experimental demonstrator, this distance is constant ($L_T = 0.2545$ m). Consequently, significant differences arise between the moments measured during the experiment and those calculated in the simulation, as shown in Fig. 11b.

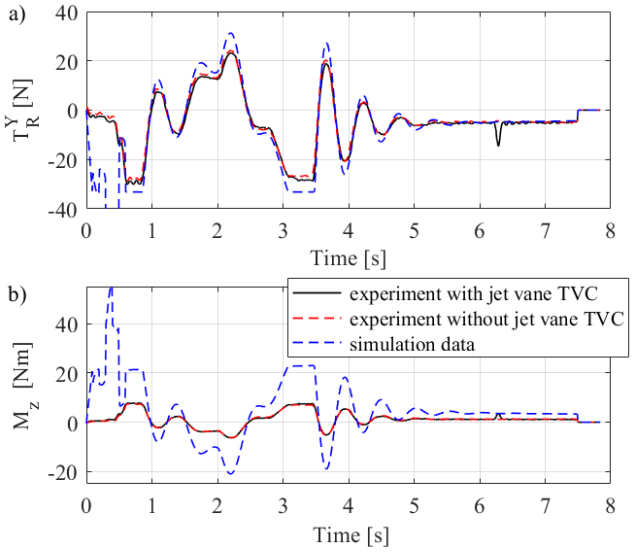

Fig. 11. Measurement results obtained at a pressure of 0.8 MPa: (a) y-component of the thrust vector, $\mathbf{T}_R^Y$, being the control force generated perpendicular to the longitudinal axis of the demonstrator; (b) moment about the z-axis, $\mathbf{M}_Z$

Figure 11 presents a comparison of experimental and simulated data for the control forces (Fig. 11a) and the moments of force about the z-axis (Fig. 11b).

To enable an objective comparison between the computer simulation results and the experimental measurements, a correction factor v was introduced. This factor accounts for the difference in the force application arm between the moving center of mass in the simulation (x_{Sm}) and the fixed distance from the pivot point to the sensor measurement location (L_T). The correction factor v is defined as follows:

$$v = \frac{L_M - x_{Sm}}{L_T} = \frac{f(t)}{L_T}. \tag{3}$$

After applying the correction factor v, which adjusts the effective moment arm (i.e., the position vector), the resulting force moments are referenced to the same pivot point and act over the same moment arm (Fig. 12).

Figure 12 presents a comparison of force moments obtained from the experiment and the simulation, recalculated with respect to a shifted measurement point to ensure comparable moment arms. As shown in the figure, the experimental moments are lower, which is attributed to the efficiency of the thrust vector deflection system. Efficiency coefficients were determined for both configurations, with and without jet vanes.

Attempts were made to derive these coefficients from simulation and experimental data. However, especially for values near

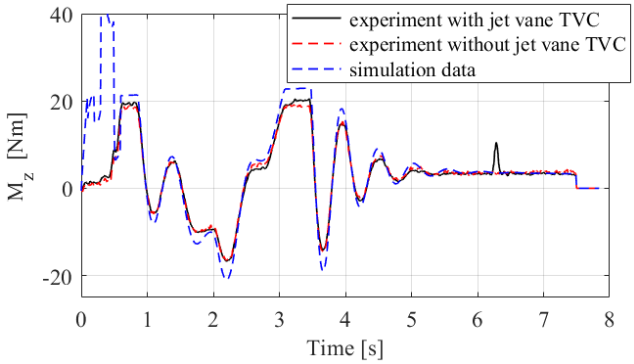

Fig. 12. Force moments referenced to the same pivot point (measurement point), with a relatively consistent moment arm

zero, the results proved unreliable. Measurement noise combined with low signal amplitudes resulted in a wide scatter of calculated efficiency values, ranging from −0.2 to over 10, clearly without physical meaning. Additional signal filtering prior to calculations did not produce satisfactory improvements. Therefore, an alternative approach was adopted, as described below.

Figure 13 shows a comparison of the control angles extracted from the simulation (δ_y) with the angles realized during the experiment. Significant differences can be observed between the commanded angle ($\delta_y \approx \delta_d$) and the angles derived from the experimental data ($\delta_v = \text{atan}\left(T_R^Y / T_R^X\right)$). It is evident that the deflection of the thrust vector actuation control system (UWS) does not align with the deflection of the resultant thrust vector. This suggests the existence of a thrust vector deflection efficiency coefficient, which represents the ratio between the actual deflection angle of the resultant thrust vector and the commanded deflection via UWS. In computer simulations, this coefficient can be used to refine and improve the mathematical model. In this paper, we estimate these coefficients using single-run data from Experiment 1.

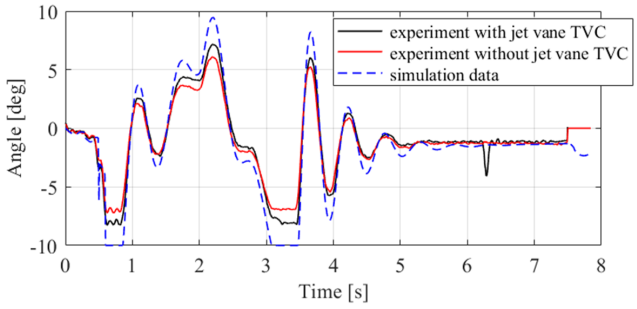

Fig. 13. Experimental and simulation thrust deflection angle

Figure 13 presents a comparison of the actual thrust deflection profiles for both the system with jet vanes and the deflection nozzle alone, alongside the theoretical deflection angle of the actuation system obtained from ATGM flight simulations. As mentioned previously, the thrust deflection angle does not exactly equal the actuation system deflection angle assumed in the simulation. To enhance the simulation fidelity, efficiency coefficients k_v and k_w, which quantify the thrust deflection effectiveness, were determined. A linear dependency was assumed

$$\delta_{jy}(t) \simeq k_j \delta_y(t), \tag{4}$$

$$\delta_{wy}(t) \simeq k_w \delta_y(t), \tag{5}$$

where δ_{jy} – thrust deflection angle in the experiment with jet vanes; δ_{wy} – thrust deflection angle in the experiment without jet vanes.

The coefficients were identified via numerical optimization using the Nelder-Mead algorithm, with the objective function defined as the integral of the squared error (ISE), as given by equations (6) and (7). For the purposes of the optimization algorithm, the equations were approximated using Euler's method

$$\text{ISE}_j = \int_0^{t_i} \left(\delta_{jy} - k_j \delta_y\right)^2 \mathrm{d}t, \tag{6}$$

$$\text{ISE}_w = \int_0^{t_i} \left(\delta_{wy} - k_w \delta_y\right)^2 \mathrm{d}t, \tag{7}$$

where t_i – the integration time (90% of the experimental duration, chosen to avoid disturbances resulting from flow cutoff).

Also, simulation-experiment errors for TCV with jet vanes and without jet vanes are defined, respectively:

$$e_j = \delta_{jy} - k_j \delta_y\,, \tag{8}$$

$$e_w = \delta_{wy} - k_w \delta_y\,. \tag{9}$$

Table 1 summarizes the parameter values before and after optimization. Figures 14 and 16 compare the experimental and simulation data while incorporating the efficiency coefficients k_j and k_w, respectively. It is also noteworthy that the quality index, namely the integral of the absolute error (IAE), was examined to assess its impact on the fitting; essentially, an almost identical fit was obtained as with the ISE index.

Table 1
Comparison of ISE and coefficient before and after optimization

Before (Fig. 13)	ISE	Coeff.
With jet vane TVC	44.8263	$k_j = 1$
Without jet vane TVC	80.6994	$k_w = 1$

After (Fig. 14 and 16)	ISE	Coeff.
With jet vane TVC	7.9277	$k_j = 0.7801$
Without jet vane TVC	5.3388	$k_w = 0.6857$

As evidenced by the graphs in Figs. 14 and 16, the obtained profiles are in significant agreement, indicating that, for our demonstrators, both with and without jet vanes, a linear relationship exists between the actuation system deflection and the thrust vector deflection. Consequently, future simulations

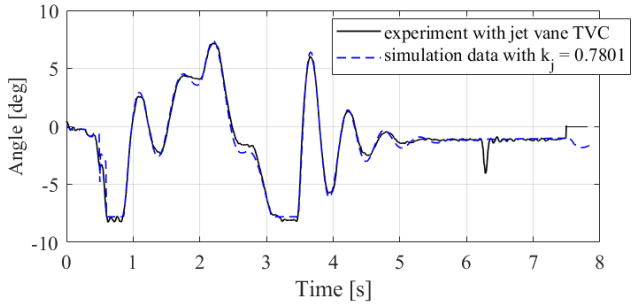

Fig. 14. Thrust deflection angle comparison of simulation results with incorporated coefficient k_j and experiment with jet vanes

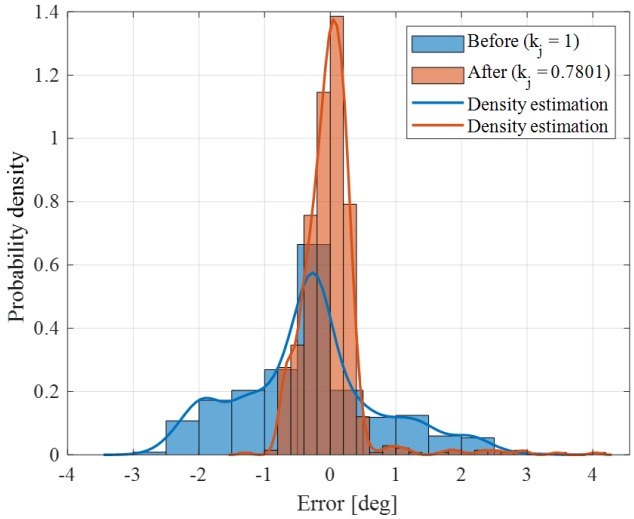

Fig. 15. Normalized histogram and density estimation of simulation-experiment with jet vanes error before and after efficiency coefficient optimization

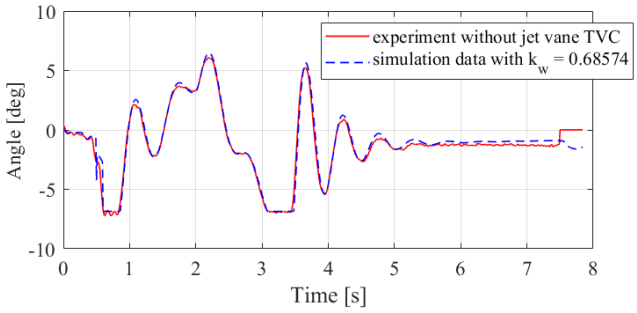

Fig. 16. Thrust deflection angle comparison of simulation results with incorporated coefficient k_w and experiment without jet vanes

may incorporate this coefficient, thereby enhancing their resemblance to real-world behavior. Additionally, the configuration with jet vanes exhibits higher efficiency, which could potentially be further improved, for instance, by optimizing the profile, shape, and material of the vanes. Also, there are no additional dynamic effects between the control system angle and thrust angle, although we observe that faster response servomotors would improve performance during rapid direction changes.

Figures 15 and 17 with normalized histogram and density estimation clearly show that for both cases (with and without jet vanes), the use of the efficiency coefficients significantly brings the error distribution closer to 0.

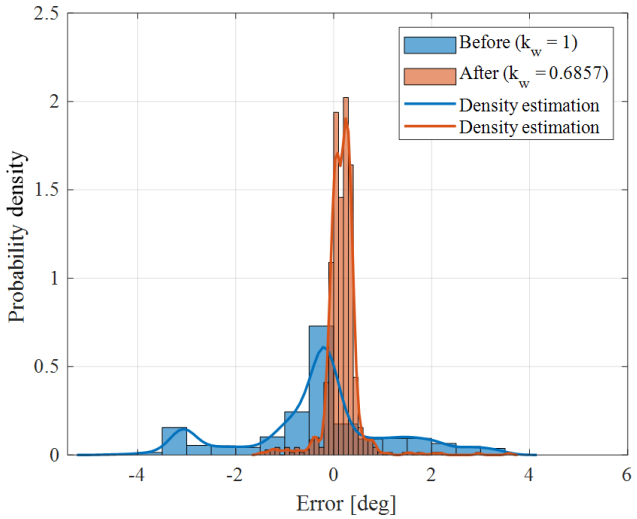

Fig. 17. Normalized histogram and density estimation of simulation-experiment without jet vanes error before and after efficiency coefficient optimization

Figure 18 illustrates the thrust generated during the experiments conducted with the demonstrator equipped with jet vanes and without jet vanes, at an inlet pressure of 0.8 MPa.

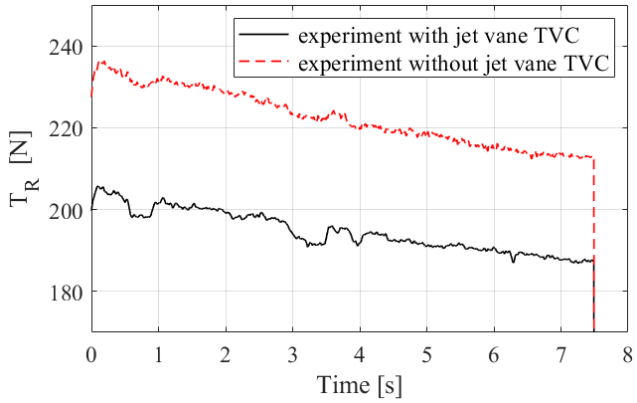

Fig. 18. The thrust vector, for the demonstrator with and without jet vanes (black solid and red dashed lines, respectively), subjected to a pressure of 0.8 MPa

Table 2 presents the fundamental statistical parameters describing the difference (error) between simulation and experimental results, both before and after the optimization of the thrust vector deflection efficiency coefficients. Although these statistics are informative, it should be noted that normality tests did not confirm a clear Gaussian distribution of the error data. The reported metrics include the mean error (in degrees), standard deviation (STD), and root mean square error (RMSE). Following the optimization process, the RMSE was reduced by

57.95% for the configuration with jet vanes and by 74.29% for the configuration without jet vanes, indicating a substantial improvement in model accuracy. Preliminary analysis suggests that the better fit observed in the configuration without jet vanes is likely due to the simpler gas deflection mechanism, which involves only the nozzle without additional aerodynamic surfaces and mechanical nonlinearities in the system.

Table 2
Error statistics before and after optimization

With jet vanes	Before	After
Mean, deg.	–0.32065	2.6749e-05
RMSE	1.1238	0.47262
STD	1.0779	0.47295

Without jet vanes	Before	After
Mean, deg.	–0.29318	0.1651
RMSE	1.508	0.38767
STD	1.4803	0.35101

4.2. Experiment 2

The other simulation results, presented in Figs. 19 and 20 concern the missile flight for the following parameters: starting target position: $x_{t0} = 1700$ m, $y_{t0} = 2$ m, $z_{t0} = 0$ m; angle of a missile launch: $\gamma_{m0} = 0$ deg, $\chi_{m0} = 0$ deg; starting angle of pitch and yaw of a target velocity vector: $\gamma_{t0} = 0$ deg, $\chi_{t0} = 0$ deg; target velocity: $V_t = 20$ m/s. Missile passing through three waypoints: $P_1(300; 7; 0)$, $P_2(900; 7; 0)$, $P_3(1300; 15; 0)$.

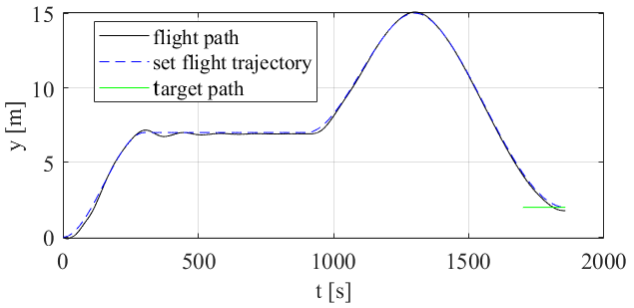

Fig. 19. The performed and set flight trajectory in the vertical plane

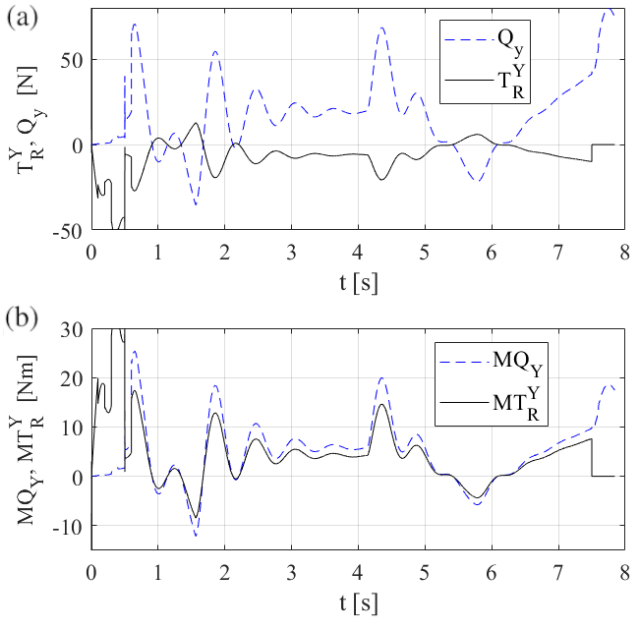

Fig. 20. The performed control forces (a) and moments (b) of the anti-tank guided missile simulated flight in the vertical plane

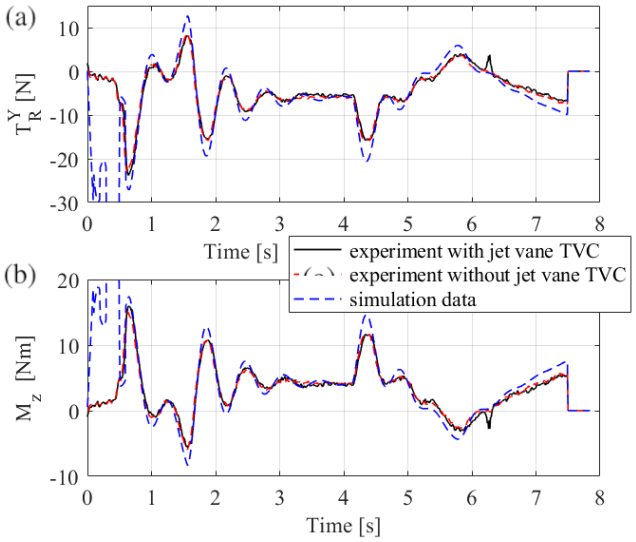

Fig. 21. Measurement results obtained at a pressure of 0.8 MPa: (a) y-component of the thrust vector, $\mathbf{T}_R^Y$, being the control force generated perpendicular to the longitudinal axis of the demonstrator; (b) moment about the z-axis, $\mathbf{M}_Z$

Based on the computer simulation performed for Experiment 2, the thrust deflection angles were extracted and implemented into the demonstrator control system.

The experimental measurements presented in Figs. 21–23 account for the previously introduced angular efficiency coefficients k_j and k_w, as well as the force arm correction factor v. Figure 21 shows a comparison between the experimental and simulation data for control forces (Fig. 21a), and the converted experimental results for the control force moments (Fig. 21b).

Figures 22 and 23 present the resultant thrust vector angles calculated from the experimental data, compared with the control angles obtained from the simulation, scaled by the angular efficiency coefficients k_j and k_w, respectively.

Figure 24 illustrates the thrust generated during the experiments conducted with the demonstrator equipped with jet vanes and without jet vanes, at an inlet pressure of 0.8 MPa. A significant difference between the measured values is clearly visible. This results from the reduction in cross-sectional area caused by the insertion of jet vanes inside the diffuser, leading to increased flow resistance for the exhaust gas stream. While the use of jet vanes positively influences the angular efficiency coefficient,

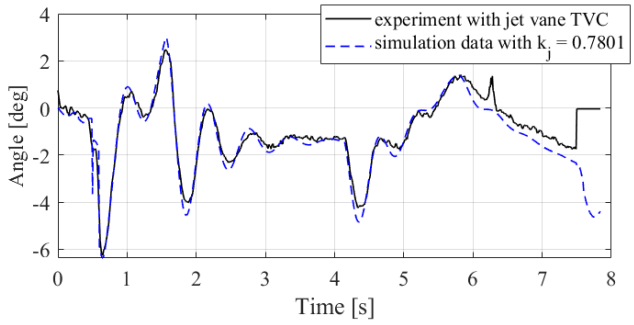

Fig. 22. Thrust deflection angle comparison of simulation results with incorporated coefficient k_j and experiment with jet vanes

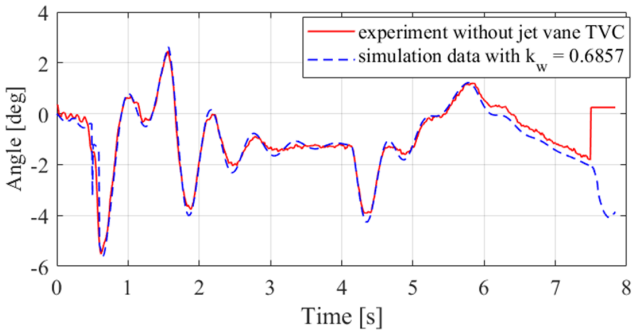

Fig. 23. Thrust deflection angle comparison of simulation results with incorporated coefficient k_w and experiment without jet vanes

it simultaneously reduces engine thrust and, consequently, the available control forces.

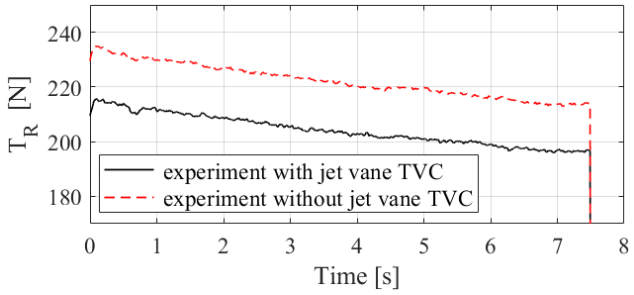

Fig. 24. The thrust vector, for the demonstrator with and without jet vanes (black solid and red dashed lines, respectively), subjected to a pressure of 0.8 MPa

As in the previous case, the key statistical parameters for Experiment 2 are summarized in Table 3. The k_j and k_w efficiency coefficients identified in Experiment 1 were applied without further adjustment. The observed reduction in RMSE, i.e., 57.64% for the configuration with jet vanes and 67.51% for the configuration without jet vanes, along with improvements in other statistical metrics, confirms that these coefficients enhance the model predictive accuracy. While it is theoretically possible to derive more statistically optimal coefficients by analyzing the distribution of best-fit values across a larger set of experiments, the incorporation of these initial coefficients already yields a substantial improvement in simulation model fidelity. This issue will be explored in future work, including potential model extensions if a nonlinear relationship proves more appropriate. It is also worth noting that incorporating efficiency factors into future simulations is expected to result in the actuator system operating more frequently at maximum deflection to maintain the desired flight trajectory.

Table 3
Error statistics for Experiment 2 before and after using coefficients from Experiment 1

With jet vanes	Before	After
Mean, deg.	–0.41426	–0.0027093
RMSE	0.75066	0.31798
STD	0.62645	0.31819
Without jet vanes	**Before**	**After**
Mean, deg.	–0.4833	–0.003678
RMSE	0.87743	0.28508
STD	0.73284	0.28526

5. FINAL CONCLUSIONS, DIRECTION OF FURTHER STUDIES

This study successfully compared simulation results of a hypothetical ATGM using a hybrid control system with experimental data from a physical TVC actuator demonstrator. The findings indicate that the TVC demonstrator effectively generates control forces and moments corresponding to the commanded deflection angles derived from flight simulations. However, a discrepancy exists between the commanded mechanical deflection and the effective thrust vector deflection, which can be characterized by linear efficiency coefficients. Specifically, the efficiency coefficient is approximately $k_j \approx 0.78$ when using jet vanes and $k_w \approx 0.69$ without vanes at a pressure of 0.8 MPa. The presence of jet vanes increases the thrust deflection efficiency ($k_j > k_w$), although it may slightly reduce the overall thrust magnitude, particularly at larger deflection angles. Additionally, an important consideration is the difference in moment calculation reference points, as the simulation accounts for a moving center of mass, whereas the experiment relies on a fixed sensor location. Properly addressing this discrepancy is important for an accurate comparison between numerical and experimental results.

While the presented results demonstrate a promising alignment between simulations and experimental data at the laboratory scale, several limitations must be acknowledged when considering real-world applications. The current model relies on simplified assumptions, such as linear efficiency scaling and quasi-steady flow behavior, which may not fully capture complex, nonlinear aerodynamic and gas-dynamic phenomena occurring at full scale or under transient conditions. Moreover, the experimental setup, though effective for initial validation, operates under controlled conditions with cold gas and static test

configurations. Translating the approach to a full-scale ATGM system would require addressing issues like high-temperature material behavior, structural loads under flight conditions, actuator robustness, and integration with guidance and navigation systems.

Future research will focus on several key areas. One priority is expanding the test rig to include real-time measurement of the physical deflection angle of the actuator system. This enhancement would enable compensation for potential servomechanism errors and allow for a more precise analysis of the relationship between the mechanical angle and the thrust deflection angle. Further investigation into the efficiency coefficients of the TVC system under varying operating pressures and flow conditions is also necessary, potentially leading to a more advanced model if simple linear scaling proves insufficient. Another significant step is conducting tests with hot gas generation to more accurately replicate actual rocket motor conditions. Lastly, optimizing the design of the jet vanes by refining their shape, profile, and material could improve deflection efficiency while minimizing thrust losses, thereby enhancing overall system performance.

REFERENCES

[1] M.S.R.C. Murty, M.S. Rao, and D. Chakraborty, "Numerical simulation of nozzle flow field with jet vane thrust vector control", *J. Aerosp. Eng.*, vol. 224, pp. 541–548, 2009, doi: 10.1243/09544100JAERO677.

[2] M.S.R.C. Murty and D. Chakraborty, "Numerical Characterisation of Jet-Vane based Thrust Vector Control Systems," *Def. Sci. J.*, vol. 65, no. 4, pp. 261–264, 2015, doi: 10.14429/dsj.65.7960.

[3] D. Daljit Majil, M. Saleem, and S. Kumaresan, "Computational study on reduction of thrust loss in jet vane thrust vectoring nozzle," *Int. J. Aerosp. Mech. Eng.*, vol. 3, no. 5, pp. 1–6, 2016.

[4] W.-H. Kim, J.-Ch. Bae, S.-T. Lim, and S.-H. Park, "Jet vane thrust vector control system," U.S. Patent US007313910B2, Jan. 1, 2008.

[5] C.S. Shin and H.D. Kim, "A Fundamental Study of Thrust-Vector Control Using a Dual Throat Nozzle," *Proc. Spring Conference 2010 of the Korean Society of Propulsion Engineering*, 2010, pp. 339–342.

[6] R. Chouicha, M. Sellam, and S. Bergheul, "Effect of chemical reactions on the fluidic thrust vectoring of an axisymmetric noz zle," *Int. J. Aviat. Aeronaut. Aerosp.*, vol. 5, no. 5, pp. 1–15, 2019, doi: 10.15394/ijaaa.2019.1377.

[7] S. Forde, M. Bulman, and T. Neill, "Thrust augmentation noz zle (TAN) concept for rocket engine booster applications," *Acta Astronaut.*, vol. 59, pp. 271–277, 2006, doi: 10.1016/j.actaastro.2006.02.052.

[8] E. Resta, R. Marsilio, and M. Ferlauto, "Thrust Vectoring of a Fixed Axisymmetric Supersonic Nozzle Using the Shock-Vector Control Method," *Fluids*, vol. 6, p. 441, 2021, doi: 10.3390/fluids6120441.

[9] V. Zmijanovic, V. Lago, L. Léger, E. Depussay, M. Sellam, and A. Chpoun, "Thrust vectoring effects of a transverse gas injection into a supersonic cross flow of an axisymmetric convergent divergent nozzle," *Prog. Propuls. Phys.*, vol. 4, pp. 227–256, 2013, doi: 10.1051/eucass/201304227.

[10] J.J. Isaac and C. Rajashekar, "Fluidic thrust vectoring nozzles," Propulsion Division National Aerospace Laboratories (Council of Scientific & Industrial Research), Bangalore 560017, India, 2014. [Online]. Available: https://core.ac.uk/ download/pdf/151646399.pdf

[11] J. Harris and N. Slegers, "Performance of a fire-and-forget antitank missile with a damaged wing," *Math. Comput. Model.*, vol. 50, pp. 292–305, 2009, doi: 10.1016/j.mcm.2009.02.009.

[12] S.Z. Živković, M.M. Milinović, P. Stefanovic, P.B. Pavlović and N. Gligorijevic, "Experimental and simulation testing of thermal loading in the jet tabs of a thrust vector control system," *Therm. Sci.*, vol. 20. pp. 275–286. 2016, doi: 10.2298/TSC1150914208Z.

[13] Ł. Nocoń, M. Grzyb, P. Szmidt, Z. Koruba, and Ł. Nowakowski, "Control Analysis with Modified LQR Method of Anti-Tank Missile with Vectorization of the Rocket Engine Thrust," *Energies*, vol. 15, no. 1, p. 356, 2022, doi: 10.3390/en15010356.

[14] J.H.C. Rojas, R.R. Serrezuela, J.A.Q. López, and K.L.R. Perdomo, "LQR Hybrid Approach Control of a Robotic Arm Two Degrees of Freedom," *Int. J. Appl. Eng. Res.*, vol. 11, no. 17, pp. 9221–9228, 2016.

[15] A.I. Isa, M.F. Hamza, and M. Muhammad, "Hybrid Fuzzy Control of Nonlinear Inverted Pendulum System," *Bayero J. Eng. Technol.*, vol. 14, no. 2,pp. 200–208, 2019.

[16] R. Yazdanpanah, M.J. Mahjoob, and E. Abbasi, "Fuzzy LQR Controller for Heading Control of an Unmanned Surface Vessel," *Proceedings of the International Conference in Electrical and Electronics Engineering*, San Francisco, USA, Oct. 2013, pp. 23–25.

[17] N.S. Bhangal, "Design and Performance of LQR and LQR based Fuzzy Controller for Double Inverted Pendulum System," *Journal of Image and Graphics*, vol. 1, no. 3, 143–146, 2013.

[18] M. Balandat, W. Zhang, and A. Abate, "On Infinite Switched LQR Problems With State and Control Constraints," *Syst. Control Lett.*, vol. 61, no. 4, pp. 464–471, 2012.

[19] W. Zhang, "Controller Synthesis for Switched Systems Using Approximate Dynamic Programming," PhD thesis, ECE Department, Purdue University, West Lafayette, USA, 2009.

[20] W. Bużantowicz, "Tuning of a Linear-Quadratic Stabilization System for an Anti-Aircraft Missile," *Aerospace*, vol. 8, no. 2, p. 48, 2021.

[21] D. Kantubhukta, K.D. Narendra, J. Vijaychandra, B. SeshaSai, K. Vedaprakash, and S.R. Koyyana, "A Review on Cascaded Linear Quadratic Regulator Control of Roll Autopilot Missile," *International Conference on IoT based Control Networks and Intelligent Systems*, 2020, pp. 88–97.

[22] Ł. Nocoń and Z. Koruba, "Optimal Compensator for Anti-Ship Missile with Vectorization of Engine Thrust," *Appl. Mech. Mater.*, vol. 817, pp. 279–288, Jan. 2016, doi: 10.4028/www.scientific.net/amm.817.279.

[23] Ł. Nocoń and Z. Koruba, "Modifications of control actuation systems of ATGM," *Appl. Mech. Mater. – Proc. 23th Int. Conf. Engineering Mechanics*, 2017, pp. 714–717.

[24] Ł. Nocoń and Z. Koruba, "Numerical analysis of the dynamics of automatically tracked antitank guided missile using polynominal functions," *J. Theor. Appl. Mech*. vol. 54, pp. 13–25, 2016.

[25] Ł.K. Nocoń, M. Grzyb, P. Szmidt, and Ł.M. Nowakowski, "An innovative thrust vectoring system with moveable jet vanes integrated with a moveable diffuser. Measurement and analysis of selected nozzle performance parameters," *Bull. Pol. Acad. Sci.*

Tech. Sci., vol. 71, p. e148444, 2023, doi: 10.24425/bpasts.2023.148444.

[26] W. Bużantowicz and J. Pietrasieński, "Dual-control missile guidance: A simulation study," *J. Theor. Appl. Mech.*, vol. 56, no. 3, pp. 727–739, 2018.

[27] Ł. Nocoń and K. Stefański, "Impact of controller performance on the process of guiding an armour-piercing missile onto a ground-based target," *Probl. Mechatron. Armament Aviat. Saf. Eng.*, vol. 7, pp. 67–84, 2016.

[28] Z. Koruba and Ł. Nocoń, "Modified linear-quadratic regulator used for controlling anti-tank guided missile in vertical plane," *J. Theor. App. Mech.*, vol. 58, pp. 723–732, 2020, doi: 10.15632/jtam-pl/122205.

[29] M. Grzyb, Ł. Nocoń, Ł. Nowakowski, and P. Szmidt, "Rocket motor exhaust nozzle," PL Patent 241948, 13 October 2022.

[30] M. Grzyb, Ł. Nocoń, Ł. Nowakowski, and P. Szmidt, "Rocket motor exhaust nozzle," PL Patent 241949, 13 October 2022.

[31] M. Grzyb, Ł. Nocoń, Ł. Nowakowski, and P. Szmidt, "Rocket motor exhaust nozzle," PL Patent 241946, f 13 October 2022.

[32] M. Grzyb, Ł. Nocoń, Ł. Nowakowski, and P. Szmidt, "Rocket motor exhaust nozzle," PL Patent 241947, 13 October 2022.

[33] M. Grzyb, Ł. Nocoń, Ł. Nowakowski, and P. Szmidt, "Rocket motor exhaust nozzle," PL Patent 241945, 12 October 2022.

[34] M. Grzyb, Ł. Nocoń, Ł. Nowakowski, and P. Szmidt, "Rocket motor exhaust nozzle," PL Patent 241969, 17 October 2022.